The Journal of Comparative Neurology
Research in Systems Neuroscience
DOI 10.1002/cne.23678

Development of MRI-based atlases of non-human brains

Jeremy F.P. Ullmann[a,#], Andrew L. Janke[a,#], David Reutens[a], Charles Watson[b]

[a] Centre for Advanced Imaging, The University of Queensland, Brisbane, Australia.
[b] Faculty of Health Sciences, Curtin University, Bentley, Western Australia, Australia.

[#] Authors contributed equally to this work

Abbreviated Title: Development of MRI Brain Atlases

Keywords: Brain Atlas, Segmentation, MRI, Registration, Model, Ontology

Corresponding author:
Dr Charles Watson
Faculty of Health Sciences
Curtin University
PO Box U1987
Bentley WA 6845
Australia
Email: c.watson@curtin.edu.au
Office telephone: +618 9266 1640
Mobile: +61 411 600 964
Fax: +618 9222 2322

Received: Aug 06, 2014; Revised: Sep 15, 2014; Accepted: Sep 17, 2014

ABSTRACT

Brain atlases are a fundamental resource for neuroscience research. In the past few decades they have undergone a transition from traditional printed histological atlases to digital atlases made up of multiple data sets from multiple modalities, and atlases based upon magnetic resonance imaging (MRI) have become widespread. In this article we discuss the methods involved in making an MRI brain atlas, including registration of multiple data sets into a model, ontological classification, segmentation of a minimum deformation model, dissemination strategies, and applications of these atlases. Finally we discuss possible future directions in the development of brain atlases.

Abbreviations:
3D – Three-dimensional
CT – Computed Tomography
DWI – Diffusion Weighted Imaging
INCF – International Neuroinformatics Coordinating Facility
MRI – Magnetic Resonance Imaging
SNR – Signal to Noise Ratio

INTRODUCTION

Brain atlases are fundamental resources for neuroscience research that provide crucial information on cytological features, structural locations, and ontology. Traditionally, brain atlases have been available as printed books containing high-resolution images of multiple markers, segmented line drawings, and detailed text explanations (Wullimann et al., 1996; Puelles et al., 2007; Watson and Paxinos, 2010; Paxinos and Franklin, 2013; Paxinos and Watson, 2014). These paper atlases are found in most neuroscience laboratories around the world and are among the most highly cited works in the field of neuroscience.

While paper atlases have functioned as vital anatomical references for many years, several shortcomings limit their utility. First, histological atlases are typically generated from a single brain (Puelles et al., 2007), or one brain per section plane (Paxinos and Watson, 2014). The information presented in the atlas is thus biased to the individual's anatomy and is not representative of a population. Pre-mortem differences, as a result of inter-specimen variability exist across most species and are even visible in the brains of inbred animal models such as the laboratory mouse. Variations are found in size, shape, and even significant morphological differences. For example, studies on the cerebellar folial pattern in inbred laboratory mice strains revealed significant inter-strain variation primarily due to allelic differences on three loci (Inouye and Oda, 1980; Neumann et al., 1993). Second, post-mortem changes caused by dissection to remove the brain and histological preparation creates several types of artifacts that can alter the shape and volume of the brain. The steps in histological processing (fixation, embedding, sectioning, and staining) also modify the tissue by causing shrinkage, stretching and tearing (Simmons and Swanson, 2009; Yang et al., 2012). Third, due to the time and labor involved in data collection, sections are often only presented at intervals of hundreds of micrometers (or in some cases even millimeters. Fourth, due to variation between planar sections such as different shrinkage artifacts, anatomical borders frequently do not align perfectly between sections and can differ by up to a few millimeters in an unpredictable direction (Majka et al., 2012). Finally, being two-dimensional, an inherent limitation of paper atlases is that they do not facilitate three-dimensional (3D) visualization of brain structures. Reconstructing a series of ill-corresponding two-dimensional sections into a 3D volume is difficult and prone to inaccuracy.

Over the past decade, magnetic resonance imaging (MRI) has become a powerful modality for generating detailed 3D digital atlases of the vertebrate brain. While MRI was initially and widely adopted for non-invasive human brain imaging, increases in magnetic field strength and improvements in coil design now allow a large range of species to be imaged at high resolution. These images form the basis of digital atlases that have numerous advantages over the traditional paper counterparts. Digital atlases can contain significantly more data, as they are not limited to the size or display format of printed atlases. They enable flexible ways of navigation through brain slices and can be updated dynamically as new data becomes available. MRI data are inherently 3D, and isotropic data sets can be re-sliced into any plane. Being acquired in a standardized 3D coordinate system or stereotaxic space, MRI data permit the registration of multiple individual brain maps to a single average space and can also serve as a framework for the inclusion of data from other modalities.

Advances in technology have progressively overcome most of the disadvantages initially encountered by MRI-based atlases. These included low resolution, low contrast, and limited availability of specific markers when compared to standard optical imaging. In terms of resolution, it is now possible to routinely achieve a resolution of 15 μm in *ex-vivo* mouse brain MRI images (Janke et al., 2012; Ullmann et al., 2012; Ullmann et al., 2013b; Ullmann et al., 2014). While, this still cannot match the highest resolution that can be achieved with optical microscopy, it is certainly at the level of low power microscopy. The range of contrast achievable with MRI has also improved as a result of the diverse array of MRI pulse sequences and contrast agents. Pre-clinical imaging is routinely performed using T_1-weighted (Johnson et al., 2010), T_2-weighted (Sharief and Johnson, 2006; Dorr et al., 2008; Papp et al., 2014), T_2*-weighted (Ullmann et al., 2010b; Ullmann et al., 2012; Ullmann et al., 2013b; Ullmann et al., 2014) and diffusion weighted imaging (Jiang and Johnson, 2011; Zhang et al., 2012) sequences to highlight differences in cytoarchitecture. New techniques such as susceptibility-weighted imaging (Haacke et al., 2004; Wang et al., 2014), oscillating gradient diffusion MRI (Aggarwal et al., 2012), are also continuously being developed to further detect microscopic differences in tissue composition and organization. Numerous contrast agents with different functional attributes based upon different paramagnetic elements (Gd^{3+}, Mn^{2+}, Cu^{2+}, Fe^{3+} and Cr^{6+}) also exist (see Table 1), although gadolinium based contrast agents are still primarily used for atlas creation.

Insert Table 1 about here

Another challenge for MRI-based atlases has been the ability to manage very large MRI model datasets (4GB - 12GB). Previously, this presented significant challenges for analysis and dissemination. However, increases in processing power of readily available or commodity computer hardware and the ability to disseminate atlases via the web using modern HTML5 and Adobe Flash based web interfaces have minimized this issue. Examples of such websites include those of the Allen Institute of Brain Science, The Scalable Brain Atlas (Bakker et al., 2010), the online BigBrain dataset at the Montreal Neurological Institute (Amunts et al., 2013) and other TissueStack based websites (Lin et al., 2013). Increasing speed of institutional and domestic Internet connections has greatly benefited dissemination and use of large MRI datasets.

Accompanying the development and distribution of digital atlases is the growing need for curation of data. For digital atlases to become an established and standardized tool in neuroscience research, they will require a consistent versioning scheme with static releases and a method to track and publish changes. The atlases should be made available on dedicated sites with data curation for future researchers. Multiple sites exist for this purpose such as NITRC.org, the Scalable Brain Atlas and the resources of the International Neuroinformatics Coordinating Facility (INCF) such as DataSpace.

The past few years have seen the publication of MRI-based brain atlases of a range of taxa including primates, rodents, birds, and fish (Ullmann et al., 2010b; Chuang et al., 2011; Frey et al., 2011; Johnson et al., 2012; Gunturkun et al., 2013). Typically these atlases have been created with delineation of some anatomical structures but without detailed descriptions of operational criteria for defining anatomical boundaries, thus

limiting the reproducibility of the segmentation. Nonetheless, if the volumetric MRI images on which the atlases are based are available, images from other studies can be aligned to the atlas data sets and model-based segmentation performed.

To aid the future development of atlases with high quality images and accurate, reproducible segmentation, in this communication we discuss the generation of an MRI-based brain model and ontology, the steps needed to create a detailed MRI-based atlas, and best practice for the dissemination of digital atlases.

REGISTRATION OF MULTIPLE DATA SETS

Brains exhibit individual variation, even with rigorous genetic and age matching; even in inbred strains, environmental differences may result in anatomical variation. For example, in a morphometric analysis of age and sex matched C57BL/6J mice, Badea et al. (2007) found that the coefficient of variation of the volume of different brain structures ranged from 2.9% for the deep mesencephalic reticular nucleus to 19.8% for the interpeduncular nucleus. Although these differences may be small for some structures, the level of variability is sufficient to drive the development of average models from a population of individuals representing the taxa rather than being biased to an individual.

Registration of multiple data sets is also needed to counter the unavoidable variations incurred during sample preparation and data acquisition. There are inevitable differences between identically prepared and acquired MRI or computed tomography (CT) data sets due to differential uptake of staining agents, artifacts such as those caused by air bubbles or tears during surgical extraction for *ex-vivo* imaging, and acquisition artifacts such as signal differences due to MR gradient non-linearity and B0 inhomogeneity (Fig. 1). These signal differences may result in poor contrast and hamper anatomical delineation in images from individual brains but can be accounted for by a systematic approach to average model generation (Fonov et al., 2011).

Early MR atlases were generated by linearly registering to a single representative individual, followed by manual scaling, to match the new atlas to existing reference spaces. Soon this registration process was augmented with non-linear registration in order to better the fit, the individuals now being matched to an existing model of normative anatomy. The process of analyzing the deformations required to match the individuals to the model became known as Deformation Based Morphometry (DBM).

At this point the process of iteratively fitting to an internal average and accounting for the average transformation became common (Grabner et al., 2006). While averaging of the transforms is a robust technique it has also been suggested that it is too simplistic for some cases and more complex methods, such as graph reduction are more applicable (Wu et al., 2011; Ying et al., 2014). During the evolution of the model building process multiple registration techniques have been used, most rely upon edge information (mutual information) or a form of normalized cross correlation (Evans et al., 2012).

Today, a robust atlas generation process ensures that the resulting model exhibits the average morphology and signal intensity of the input datasets. The model generation consists of an initial linear registration followed by nonlinear registration to an internally evolving average image. Non-linear registration takes into account inter-

individual differences between brains. During model generation, a "winner takes all" or robust averaging approach can be used in which voxels in the individual brain images that deviate from the current mean by more than a set amount are down-weighted. This is an effective technique to identify and remove artifacts that are not consistent between individual images.

In most cases it also beneficial to produce a symmetric (left/right) atlas. This effectively doubles the number of subjects and increases the signal to noise ratio (SNR). Symmetric atlases are also desirable for model based segmentation because it halves the time for the initial manual segmentation of the model. A symmetric atlas ensures that left-right bias is not introduced by automatic segmentation techniques that utilize non-linear registration. It can however be counter-productive if significant left-right asymmetry truly exists in individual images.

During atlas creation, parametric maps can also be generated of the residual variability in local morphology after each stage of fitting. These provide insight into which parts of the model have greatest homology and thus where a high degree of accuracy from model based segmentation can be expected. The following is an outline of the steps we have used to create an average nonlinear model.

1. *Determine the number of individuals and collect data*
Determine the number of individuals and collect data
As a rule, a larger number of individuals yields a more consistent average in model creation. However, at some point adding more individuals to a model will have diminishing gains for SNR. In general, greater pre-mortem variability in structure will require a larger number of individuals. Previous studies have shown that ~150 human subjects are required to produce a brain atlas that is representative of a population (Janke and Budge, 2009). In contrast, it has been shown that for the inbred wildtype C57BL/6J mouse only 8 brains are required (Janke et al., 2012). While there is no fixed minimum contrast to noise ratio, a reduction in contrast will require a larger number of individuals in a model to achieve a similar result. To determine the number of specimens required for a specific organism, the model building process should be monitored to ascertain the point at which adding more individuals no longer reduces the summed variance significantly (see step 5). As mentioned in the introduction, there are numerous imaging sequences that elicit different features of cytoarchitecture. However, we suggest using T2 weighted imaging as this is the most used modality in the imaging of normal mammalian brains. The selection of this modality therefore facilitates comparison with existing datasets.

2. *Pre-processing*
It is important to organize data in a standard orientation, as the model will define the space and co-ordinate system that will be referenced by others. If there no standard orientation exists, a sensible choice would be one based upon closely related taxa. For example, for the mouse the Bregma/Interaural/Flat Skull and Waxholm systems are typically used (Johnson et al., 2010; Paxinos and Franklin, 2013). Conventionally, the medial to lateral dimension is the Y plane and inferior-superior dimension is the Z plane. Care should be taken to avoid confusing the left and right hemispheres. Consideration should be given to scaling the data or provision of a transformation to match it to models of similar taxa.

Insert Figure 1 about here

Obvious artifacts, such as the results of poor dissection or extraneous cranial nerves should be masked, aiming to make all the brains in the model look as similar as possible (Figure 1). MRI data also require correction of intensity inhomogeneity; a commonly used algorithm for this is N3 (Sled et al., 1998). Gradient field mapping can also be used to account for gradient induced geometric distortion.

3. *Model generation*

A number of published techniques can be used to create minimum deformation atlases (Joshi et al., 2004; Fonov et al., 2011; Janke et al., 2012). To avoid common pitfalls, newcomers to model generation are encouraged to use an existing, validated method. The methods share the common goal of recursively fitting the individual data to an internal evolving brain model. Using a low order fitting procedure, the data are generally first fitted either to an existing model, if one is available, or to a randomly selected dataset in the subject group. This allows an initial average, termed the level 0 model, to be created. Each dataset is then fitted to the level 0 model using a more refined fitting strategy, allowing a level 1 model to be created. The process is then iterated with a progressively finer fitting strategy until a stable model is created at the desired resolution and level of fit (Figure 2). Different model creation techniques usually generate different results from the model generation phase of each iteration. The inverse of the average registration transformation from each of the individuals to the current model is commonly applied to the current model to ensure that the final result is not biased to the starting model or image. This ensures that the model reflects the average morphology of the subject group.

Insert Figures 2, 3, and 4 about here

If the number of subjects is sufficiently large, the resolution of the model can be increased as it is being created. Conceptually this is similar to signal averaging, with increased SNR due to the alignment of homologous structures in images from individual subjects. During the model creation it is also advantageous to inspect the signal averages and standard deviation images at each iteration. The standard deviation image shows sites of residual variability in the model population, with a higher local variability signifying greater residual morphometric variability in that area (Figure 3). The final standard deviation image can also be used to determine the areas of consistent structure in the cohort and thus where model-based segmentation will perform well (Figure 4). In contrast, for areas with high residual variation, nonlinear fitting to the average model will generally result in a poorer fit, resulting in inconsistent model-based segmentation of individual brain images.

4. *Model cleanup and conversion to a standard data format*

Following model creation, sampling and extent of the model need to be decided. It is important to consider how the scientific community will utilize the model. For example, it may seem attractive at this stage to crop the model to include only specific anatomical structures of interest such as the cerebellum or removing part of the spinal cord. However, cropping the data will limit the utility of the model and the accuracy of registration by other users may be reduced if there is incomplete coverage of the brain. For these reasons, it is generally best to leave 10 voxels of free space around the model.

ONTOLOGICAL DEFINITION AND CLASSIFICATION

An ontology is a way to represent an existing domain of knowledge in the form of a hierarchical taxonomy (Gruber 1993). There have in the past been a number of attempts to create a brain ontology; these include NeuroNames (Bowden and Martin, 1995; Bowden et al., 2007), the Biomedical Information Research Network (BIRN) (Bug et al., 2008), and the Brain Architecture Management System (BAMS) (Bota et al., 2005; Bota and Swanson, 2008). However, these ontologies are largely based on traditional topographic classification of parts of the adult brain, whereas the advent of gene targeting in mice (Capecchi, 1989) has had a major impact on the understanding of brain ontology (Puelles et al., 2013). Studies of progressive gene expression and lineage mapping during development have revealed the true relationships of parts of the brain, thus replacing older schemes based on topography. For example, the subthalamic nucleus is clearly a hypothalamic derivative rather than a distinct part of the diencephalon (Puelles et al., 2013). The new developmental ontology has arrived just in time to inform modern MR segmentation studies, and has already been incorporated into an MR analysis of postnatal brain development in the rat (Calabrese et al., 2013). The incorporation of modern views of ontology will greatly enhance MR studies on brain segmentation.

A PROTOCOL FOR SEGMENTATION OF MRI DATA

Segmentation of a novel MRI brain atlas set can be a daunting and difficult task. Image contrast in a variety of imaging sequences may provide subtle clues for the location of boundaries of anatomical structures. To perform the segmentation, a thorough understanding of the visible contrast and a discerning eye for distinguishing the subtleties in contrast is required. The skill set required and the steps to follow are not all that different from those for structural delineation on a conventional histological data set. The following is a step-by-step protocol for segmentation of a novel MRI data set.

1. Identify major landmarks, such as major brain regions, large fiber bundles or large nuclei, on the MRI slice to orient oneself within the brain.

2. Identify major structures that have distinct borders that can be used to anchor the rest of segmentation.

3. Begin segmentation with the ‘anchor’ structures.

4. Segment every (2^n)th slice to allow interpolation of the segmentation in intervening slices; if required the intervening slices can also be segmented. For larger structures every eighth slice may be enough while for smaller regions every second slice may be required. Only segment one side of the model if a symmetric model is used as the segmentation can be automatically mirrored during interpolation.

5. Begin to delineate other visible structures making sure to flip back and forth between MRI slices to verify borders. It is advantageous to use a symmetric model because structures on one side remain visible to aid the delineation of structures on the other side of the brain.

6. While it is usually easiest to segment in one plane, MR images in the other two orthogonal planes can provide evidence of structural boundaries not apparent in the primary orientation. Examining the segmentation in the other two orthogonal planes provides important internal validation of the evolving segmentation.

7. If an existing histological atlas exists for the same or similar species, attempt to find a section in the similar plane. Note that this can be very difficult due to difference in the angle at which the histological section was cut. As a result, more than one MRI slice may partly correspond to a single histological section, such as when the dorsal and ventral parts of a MRI slice correspond to different histological sections. This can be overcome by re-slicing the MRI data to the orientation of the histological atlas if the MRI data are isotropically sampled. However, it is important to be aware that the orientation of sections in the histological atlas may not be consistent throughout the brain.

8. Start from one end of a brain region and work towards the middle. Then stop and segment from the other end of the brain region again working towards the middle. This is a way of confirming the segmentation, as ideally the structural borders should match in the middle.

9. Finally, it is invaluable to put the segmentation aside and review it after some time. From experience, the more time spent looking at the MRI data set the greater the number of structural boundaries that will be identified.

Insert Figure 5 about here

Using this method we provide a description of the segmentation of the rostral brain stem on successive images in Figure A1-A3. Newly identified structures are in white lettering, while previously delineated structures are in black/gray lettering.

1. The rostral part of the brain stem begins with the caudal cerebellum still visible (Figure 5A1). The cerebellum, including the flocculus (Fl) and lobule 2 of the cerebellar vermis (2Cb,) and very well defined fibers tracts, including the facial nerve (7n), the vestibulocochlear nerve (8n), and the spinal trigeminal tract (sp5), provide major landmarks with which to frame the brainstem. Also visible are a few additional white matter structures from the cerebellum including the superior cerebellar peduncle (scp) and the uncinate fasciculus of the cerebellum (un).
2. With more careful examination of the brain stem it is possible to begin to delineate less obvious structures (Figure 5A2). This includes hypointense fiber tracts medial longitudinal fasciculus (mlf), the pyramindal tract (py), the rubrospinal tract (rs), and the ventral spinocerebellar tract (vsc). Hyperintense structures also become more apparent including the olivocochlear bundle (ocb) and the nucleus of the trapezoid body (Tz). Lateral to Tz, three slightly less hyperintense nuclei (when compared to Tz) are separated by a hypointense border including the more medial superior paraolivary nucleus (SPO), the lateral superior olive (LSO), and the ventrally located medioventral periolivary nucleus (MVPO).
3. Finally, a few general borders of a few nuclei can be ascertained based upon the previously identified structures (Figure 5A3). These include the hypointense dorsal periolivary region (DPO) that lies dorsal to LSO; the intermediate reticular nucleus (IRT) which is lies medially to 7n and lateral to the slightly darker

pontine reticular nucleus (PnC); ventro-medial to PnC is the lighter gigantocellular reticular nucleus (GiA), and surrounding the raphe the hypointense raphe magnus nucleus (RMg).

Another approach, which we are not keen to recommend in most cases, is to conduct 'automatic' segmentation of MR images by the direct application of histological data to the MR images. To do so, direct correspondence between the two data sets needs to be established by digital reconstruction of the histological data set and registration of the histological data to MRI data. Depending on the availability of histological data two methods are possible. The first method entails registering an established histological atlas to the MRI data using either manual landmark or point based registration or automated mutual information registration (Collignon et al., 1995). Registration can be performed on histological sections or line figures created from the histological data. The main advantage of using a published atlas is that data are likely to be of high quality and already accepted by the scientific community. However, even the best histological atlases have structural borders that do not align perfectly between sections. As a result, the reconstructed borders of brain regions can appear very jagged in the planes orthogonal to the plane of histological sectioning. A second method is to perform histology on a brain that has been imaged with MRI. Using an iterative process, MRI slices are matched to the histological sections followed by a piecewise rigid registration (Yang et al., 2012).

Insert Figure 6 about here

Registration of the MRI model to a histology-based segmentation allows direct correlation of anatomical boundaries visible on MRI and on histological features. For example in Figure 6 we can correlate the medial lemniscus between the individual MRI data set (Figure 6 bottom) and its corresponding restacked histological data set (Figure 6 top). The difficulty of collecting and aligning histological sections to MRI data should not be underestimated. Ideally, every histological section needs to be collected and histology is almost impossible to do perfectly. Moreover, nonlinear tissue distortions including rolling or separating of sections, shrinkage that occurs during staining and mounting, and intensity inhomogeneities due to uneven staining all hinder the reconstruction and registration processes. Nonetheless, if an excellent histological series can be collected, reconstruction and registration methodologies can be automated and amenable to high throughput.

DISSEMINATION STRATEGIES

Dissemination of brain atlases is the final essential aspect of atlas creation. The sharing of data and segmentations will accelerate progress in the fundamental understanding of a brain. Importantly, it reduces the cost of subsequent studies by obviating unnecessary manual segmentation. Sharing of brain models also enables standardization and the use of common reference co-ordinate frame, facilitating the description and understanding of research findings and allowing future meta-analysis of large agglomerated data sets. Data sharing is also a method of enhancing accountability for the published work, permitting scrutiny of the source data. Inevitably, all brain atlases are based on imperfect primary images (*e.g.* noise, missing data, etc.) and data sharing facilitates quality improvement by enabling others to discover and remedy errors and by allowing iterative updating as new data become available.

However, dissemination of data faces a number of obstacles. Typically, researchers have created their own websites where data are accessible for download. However, these websites are often unstable and may only be maintained for the limited time due to constraints of funding, manpower, server infrastructure and location of the researcher and research group. Moreover, it is time consuming and often difficult to keep up to date with changes in operating system, visualization software, server security patching and other administrative tasks. More generalized websites such as The Neuroscience Information Framework (http://neuinfo.org) and Databib (http://databib.org) often provide lists of various atlases but typically these are also incomplete.

The most mature field in this area is that of human brain imaging. The International Consortium for Brain Imaging (ICBM) was specifically established for the purpose of creating and disseminating atlases of human cortical structure. In the ICBM's case dedicated and managed websites are used (http://loni.usc.edu/ICBM/) that allow continued access to the data now 20 years after the inception of the Consortium. Other sites such as NITRC (www.nitrc.org) have also emerged as possible repositories offering free long term storage and data curation in a location with which many are already familiar or already actively searching for data. Addressing the issues of maintaining atlases in this area, we provide the following recommendations when disseminating new MRI-based atlases.

1. Resist the urge to release the model immediately.
2. Decide on a naming scheme early. Use other atlases that have already been released for guidance here. The Paxinos/Watson nomenclature and abbreviation set (Paxinos and Watson, 1982) has become the most widely used in the field of neuroscience, and has been adopted by almost all major mammalian and avian brain atlases (Morin and Wood, 2001; Paxinos et al., 2007; Puelles et al., 2007; Ashwell and Paxinos, 2008; Mai et al., 2008; Paxinos et al., 2009a; Paxinos et al., 2009b; Watson and Paxinos, 2010; Paxinos et al., 2012; Paxinos and Franklin, 2013; Paxinos and Watson, 2014).
3. Ensure the data are in a well-recognized or documented coordinate space.
4. Decide on a version numbering system and license for the model and only release data with a version number and license. Once a release has been made, be sure to archive a local copy of the release for future reference. It is likely that changes and updates will be required over time and a method to track these is essential.
5. Provide metadata. Metadata should include descriptions of the content of the data, its file format, sample source, preparation methods, data acquisition strategy, field strength, filters and other associated data. It is also critical to include the provenance of any post processing and segmentation. Data must be in a format that other researchers can clearly understand and use. Provisos for open or limited use of the data should be made clear by clearly stipulating conditions such as restricting useto non-commercial applications.. A commonly used and well understood method of defining and documenting re-use rights is by giving the data a Creative Commons, BSD, or GPL license.
6. Decide where the data will be deposited and hence from where it will be released. Currently, good choices here include INCF, Dryad, and GitHub. While GitHub is not primarily designed for the release of data, it is a good repository with well-

established versioning history tools for the release of metadata and software code that can accompany the data.

PHENOTYPING USING MRI-BASED ATLASES

The free dissemination of brain atlases enables researchers around the world the ability to assess novel models of neurological disease. Using a deformation based morphometry (DBM), MR images from a disease model are non-linearly registered to a common coordinate space and then the inverse transformation fields are applied to an established atlas to automatically segment the disease model brains into individual regions. DBM has been extensively applied to human MRI data, but only recently been utilized in non-human imaging experiments. With the more recent development of numerous rodent atlases automated image-processing tools (Budin et al., 2013; Ma et al., 2014) rapid phenotyping of mouse models is also possible. As a result, DBM has now also been utilized in examining mouse models autism (Horev et al., 2011; Steadman et al., 2014), fragile X syndrome (Ellegood et al., 2010) Huntington disease (Carroll et al., 2011), Alzheimer's disease (Badhwar et al., 2013), and depression (Spinelli et al., 2013).

INTEGRATION OF STRUCTURE AND FUNCTION

Bridging the gap between structural and functional imaging is the next goal in neuroscience research. Numerous methods, that cover a range of scales, exist for functional analyses. At the cellular level these include genetic approaches such as examinations of immediate early genes, whose expression is upregulated with neuronal activity (Sheng and Greenberg, 1990; Guzowski et al., 2005), and calcium imaging and optogenetics which enable visualization and manipulation of activity in defined cell types (Stosiek et al., 2003; Tian et al., 2009; Lim et al., 2013). At the whole-brain level the two most widely used techniques are manganese-enhanced magnetic resonance imaging (MEMRI) and functional magnetic resonance imaging (fMRI). MEMRI exploits characteristics of manganese: paramagnetism, a calcium analog, and transportation along axons and across synapses to neighboring neurons (for review see (Inoue et al., 2011) to visualize brain activity while fMRI detects changes in blood flow or the blood-oxygen level as a proxy for neuronal activity. Brain atlases are fundamental to these techniques as they facilitate examinations of brain function by 1) serving as templates spaces for the registration of new data (Johnson et al., 2010; Frey et al., 2011; Ku et al., 2011; Papp et al., 2014), and 2) segmentation of whole-brain functional data sets into individual structures or regions of interest to deduce areas of brain activation (Valdes-Hernandez et al., 2011; Belcher et al., 2013; Miranda-Dominguez et al., 2014; Sforazzini et al., 2014). For example, registration of MEMRI data to an existing MRI atlas enabled identified reduced brain activity in the amygdala and hippocampus in a mouse model of human tauopathy (Perez et al., 2013).

Despite the widespread use of these various techniques there is a clear need to develop a better understanding of how different mapping modalities, at different spatial and temporal scales relate to one another, given the assumptions underlying these measurements and sources of noise and error. As a result, more recently there has been an effort to combine modalities at the various scales including validation of MEMRI with immediate early gene expression (Malkova et al., 2014) and combined optogenetic-fMRI experiments (Lee et al., 2010; Desai et al., 2011; Gerits et al.,

2012). While these combinations have been successful, they still do not overcome the fundamental problem in multi-scale analyses - that statistical analysis techniques have been developed to control for significance given the unique characteristics of the data in each specific modality. In most cases this means that spatial smoothing constraints have to be introduced to the data, most typically in MRI. In doing this a researcher is limited to only analyzing data from a particular scale as other data would have to be either up or down-sampled to be included, thus loosing its utility. Novel techniques for the statistical estimation significance via FDR (False Discovery Rate) have recently been proposed in (Nguyen et al., 2014) that do not require an a-priori estimation of effect size and thus define a way in which the combined statistical analysis of data from multiple scales could be achieved.

FUTURE DIRECTIONS

Since the creation of early histological atlases, significant progress has been made in the development of brain maps. In the past few decades, the field has moved towards digital atlases composed of data from a group of individuals collected with a range of modalities. For example, population atlases created for many animal models now routinely include MRI, CT, diffusion weighted imaging (DWI), and histology (Johnson et al., 2010; Gunturkun et al., 2013; Ullmann et al., 2013a). Although multi-modal atlases are becoming commonplace and provide greater detail, they are limited by primarily using different imaging sequences and only some serial histology. However, recent developments in non-destructive whole-brain technologies are exciting as they introduce fewer artifacts than histological processing, and permit acquisition of high-resolution whole-brain imaging datasets. Whole brain clearing techniques (i.e. CUBIC, CLARITY and SeeDB) at the light microscope level preserve the fine morphological architecture of the brain enabling the collection of whole-brain immunohistochemistry data (Chung et al., 2013; Ke et al., 2013; Susaki et al., 2014). In doing so, they permit the interrogation of the brain from a gene or protein level all the way to a whole brain connectivity level. At the nanostructural level, techniques for staining and embedding the whole mouse brain have also been developed (Mikula et al., 2012). When combined with serial block-face electron microscopy these methods present the possibility of increasing the resolution of brain maps to the 10 – 100 nm scale (Kleinfeld et al., 2011).

Concurrent developments in image analysis and computer processing power make the creation of population based CLARITY or SeeDB atlases feasible. However, significant hurdles with registration of such high-resolution and detailed data sets must first be overcome before this can be achieved. Massive data storage and processing power is required to perform automated registration on the substantial amounts of data generated by these new technologies. Algorithms to deal with the non-isotropic data generated by light microscopy must be developed. Data from light microscopes is always of lower resolution in the Z-plane due to the point spread function. The breakdown of homology between scales also poses a challenge. A fundamental assumption when averaging data at the level of MRI, CT and positron emission tomography is that sufficient homology exists at the scale of image acquisition to allow the statistical approach of averaging data from multiple subjects to be well posed. At the resolution of optical microscopy and ultrastructure, it is not readily apparent that this assumption holds. Consequently, novel algorithms and statistical techniques need to be developed to both extract consistent microstructural features from and achieve registration of multiple data sets a these high resolutions.

Finally, future brain maps will need to move beyond structural maps to incorporate correlated structure/function maps. At present this is limited to organisms with transparent brains (*i.e.* zebrafish) where optical technologies permit visualization of near simultaneous behavior and neuronal activity. However, we anticipate that recent large-scale initiatives such as the National Institute of Health funded Brain Research through Advancing Innovative Neurotechnologies (BRAIN) project will transform our experimental capabilities in this domain.

ACKNOWLEDGEMENTS

All authors had full access to all the data in the study and take responsibility for the integrity of the data and the accuracy of the data analysis. Study concept and design: JU, AJ, CW. Acquisition of data: JU, AJ. Analysis and interpretation of data: JU, AJ, DR. Drafting of the manuscript: JU, AJ. Critical revision of the manuscript for important intellectual content: CW, DR. Study supervision: DR, CW.

REFERENCES

Aggarwal M, Jones MV, Calabresi PA, Mori S, Zhang J. 2012. Probing mouse brain microstructure using oscillating gradient diffusion MRI. Magn Reson Med 67:98-109.

Amunts K, Lepage C, Borgeat L, Mohlberg H, Dickscheid T, Rousseau ME, Bludau S, Bazin PL, Lewis LB, Oros-Peusquens AM, Shah NJ, Lippert T, Zilles K, Evans AC. 2013. BigBrain: an ultrahigh-resolution 3D human brain model. Science 340:1472-1475.

Angenstein F, Niessen HG, Goldschmidt J, Lison H, Altrock WD, Gundelfinger ED, Scheich H. 2007. Manganese-enhanced MRI reveals structural and functional changes in the cortex of Bassoon mutant mice. Cereb Cortex 17:28-36.

Ashwell K, Paxinos G. 2008. Atlas of the Developing Rat Nervous System. San Diego: Elsevier Academic Press.

Badea A, Ali-Sharief AA, Johnson GA. 2007. Morphometric analysis of the C57BL/6J mouse brain. NeuroImage 37:683-693.

Badhwar A, Lerch JP, Hamel E, Sled JG. 2013. Impaired structural correlates of memory in Alzheimer's disease mice. NeuroImage Clinical 3:290-300.

Bakker R, Larson SD, Strobelt S, Hess A, Wojcik D, Majka P, Kotter R. Scalable Brain Atlas: From Stereotaxic Coordinate to Delineated Brain Region. Frontiers in Neuroscience. Conference Abstract: Neuroinformatics 2010, Kobe, Japan. DOI: 10.3389/conf.fnins.2010.13.00028.

Belcher AM, Yen CC, Stepp H, Gu H, Lu H, Yang Y, Silva AC, Stein EA. 2013. Large-scale brain networks in the awake, truly resting marmoset monkey. J Neurosci 33:16796-16804.

Blackwell ML, Farrar CT, Fischl B, Rosen BR. 2009. Target-specific contrast agents for magnetic resonance microscopy. NeuroImage 46:382-393.

Bota M, Dong HW, Swanson LW. 2005. Brain architecture management system. Neuroinformatics 3:15-48.

Bota M, Swanson LW. 2008. BAMS Neuroanatomical ontology: design and implementation. Front Neuroinform 2:2.

Bowden DM, Dubach M, Park J. 2007. Creating neuroscience ontologies. Method Mol Biol 401:67-87.

Bowden DM, Martin RF. 1995. NeuroNames Brain Hierarchy. NeuroImage 2:63-83.

Budin F, Hoogstoel M, Reynolds P, Grauer M, O'Leary-Moore SK, Oguz I. 2013. Fully automated rodent brain MR image processing pipeline on a Midas server: from acquired images to region-based statistics. Front Neuroinform 7:15.

Bug WJ, Ascoli GA, Grethe JS, Gupta A, Fennema-Notestine C, Laird AR, Larson SD, Rubin D, Shepherd GM, Turner JA, Martone ME. 2008. The NIFSTD and BIRNLex vocabularies: building comprehensive ontologies for neuroscience. Neuroinformatics 6:175-194.

Calabrese E, Johnson GA, Watson C. 2013. An ontology-based segmentation scheme for tracking postnatal changes in the developing rodent brain with MRI. NeuroImage 67:375-384.

Capecchi MR. 1989. The new mouse genetics: altering the genome by gene targeting. Trends Genet 5:70-76.

Caravan P. 2006. Strategies for increasing the sensitivity of gadolinium based MRI contrast agents. Chem Soc Rev 35:512-523.

Caravan P, Ellison JJ, McMurry TJ, Lauffer RB. 1999. Gadolinium(III) chelates as MRI contrast agents: structure, dynamics, and applications. Chem Rev 99:2293-2352.

Carroll JB, Lerch JP, Franciosi S, Spreeuw A, Bissada N, Henkelman RM, Hayden MR. 2011. Natural history of disease in the YAC128 mouse reveals a discrete signature of pathology in Huntington disease. Neurobiol Dis 43:257-265.

Chan KC, Fan SJ, Zhou IY, Wu EX. 2012. *In vivo* chromium-enhanced MRI of the retina. Magn Reson Med 68:1202-1210.

Chuang N, Mori S, Yamamoto A, Jiang H, Ye X, Xu X, Richards LJ, Nathans J, Miller MI, Toga AW, Sidman RL, Zhang J. 2011. An MRI-based atlas and database of the developing mouse brain. NeuroImage 54:80-89.

Chung K, Wallace J, Kim SY, Kalyanasundaram S, Andalman AS, Davidson TJ, Mirzabekov JJ, Zalocusky KA, Mattis J, Denisin AK, Pak S, Bernstein H, Ramakrishnan C, Grosenick L, Gradinaru V, Deisseroth K. 2013. Structural and molecular interrogation of intact biological systems. Nature 497:332-337.

Collignon A, Maes F, Delaere D, Vandermeulen D, Suetens P, Marchal G. 1995. Comp Imag Vis 3:263-274.

Desai M, Kahn I, Knoblich U, Bernstein J, Atallah H, Yang A, Kopell N, Buckner RL, Graybiel AM, Moore CI, Boyden ES. 2011. Mapping brain networks in awake mice using combined optical neural control and fMRI. J Neurophysiol 105:1393-1405.

Dorr AE, Lerch JP, Spring S, Kabani N, Henkelman RM. 2008. High resolution three-dimensional brain atlas using an average magnetic resonance image of 40 adult C57BL/6J mice. NeuroImage 42:60-69.

Ellegood J, Pacey LK, Hampson DR, Lerch JP, Henkelman RM. 2010. Anatomical phenotyping in a mouse model of fragile X syndrome with magnetic resonance imaging. NeuroImage 53:1023-1029.

Evans AC, Janke AL, Collins DL, Baillet S. 2012. Brain templates and atlases. NeuroImage 62:911-922.

Fonov V, Evans AC, Botteron K, Almli CR, McKinstry RC, Collins DL. 2011. Unbiased average age-appropriate atlases for pediatric studies. NeuroImage 54:313-327.

Frey S, Pandya DN, Chakravarty MM, Bailey L, Petrides M, Collins DL. 2011. An MRI based average macaque monkey stereotaxic atlas and space (MNI monkey space). NeuroImage 55:1435-1442.

Frullano L, Zhu J, Wang C, Wu C, Miller RH, Wang Y. 2012. Myelin imaging compound (MIC) enhanced magnetic resonance imaging of myelination. J Med Chem 55:94-105.

Gerits A, Farivar R, Rosen BR, Wald LL, Boyden ES, Vanduffel W. 2012. Optogenetically induced behavioral and functional network changes in primates. Curr Biol 22:1722-1726.

Grabner G, Janke AL, Budge MM, Smith D, Pruessner J, Collins DL. Symmetric atlasting and model based segmentation : an application to the hippocampus in older adults. Medical Image Computing and Computer-Assisted Intervention MICCAI, Part II. 2006. pp. 58–66

Gunturkun O, Verhoye M, De Groof G, Van der Linden A. 2013. A 3-dimensional digital atlas of the ascending sensory and the descending motor systems in the pigeon brain. Brain Struct Funct 218:269-281.

Guzowski JF, Timlin JA, Roysam B, McNaughton BL, Worley PF, Barnes CA. 2005. Mapping behaviorally relevant neural circuits with immediate-early gene expression. Curr Opin Neurobiol 15:599-606.

Haacke EM, Xu Y, Cheng YC, Reichenbach JR. 2004. Susceptibility weighted imaging (SWI). Magn Reson Med 52:612-618.

Horev G, Ellegood J, Lerch JP, Son YE, Muthuswamy L, Vogel H, Krieger AM, Buja A, Henkelman RM, Wigler M, Mills AA. 2011. Dosage-dependent phenotypes in models of 16p11.2 lesions found in autism. Proc Natl Acad Sci USA 108:17076-17081.

Inoue T, Majid T, Pautler RG. 2011. Manganese enhanced MRI (MEMRI): neurophysiological applications. Rev Neurosci 22:675-694.

Inouye M, Oda SI. 1980. Strain-specific variations in the folial pattern of the mouse cerebellum. J Comp Neurol 190:357-362.

Janke AL, Budge M. ANDI - The Australian normative and dementia imaging collaborative network: tools and methods for amalgamating large neuroimaging databases. International Conference on Alzheimer's Disease. 2009; Vienna, Austria. Abstract Number P3-089.

Janke AL, Ullmann JFP, Kurniawan ND, Paxinos G, Keller M, Yang Z, Richards K, Egan G, Petrou S, Galloway G, Reutens D. 15µm average mouse models in Waxholm space from 16.4T 30µm images; Neuroinformatics 2012, Melbourne, Australia. Abstract Number P:110.

Jiang Y, Johnson GA. 2011. Microscopic diffusion tensor atlas of the mouse brain. NeuroImage 56:1235-1243.

Johnson GA, Badea A, Brandenburg J, Cofer G, Fubara B, Liu S, Nissanov J. 2010. Waxholm space: An image-based reference for coordinating mouse brain research. NeuroImage 53:365-372.

Johnson GA, Calabrese E, Badea A, Paxinos G, Watson C. 2012. A multidimensional magnetic resonance histology atlas of the Wistar rat brain. NeuroImage 62:1848-1856.

Joshi S, Davis B, Jomier M, Gerig G. 2004. Unbiased diffeomorphic atlas construction for computational anatomy. NeuroImage 23 Suppl 1:151-160.

Ke MT, Fujimoto S, Imai T. 2013. SeeDB: a simple and morphology-preserving optical clearing agent for neuronal circuit reconstruction. Nat Neurosci 16:1154-1161.

Kleinfeld D, Bharioke A, Blinder P, Bock DD, Briggman KL, Chklovskii DB, Denk W, Helmstaedter M, Kaufhold JP, Lee WCA, Meyer HS, Micheva KD, Oberlaender M, Prohaska S, Reid RC, Smith SJ, Takemura S, Tsai PS, Sakmann B. 2011. Large-scale automated histology in the pursuit of connectomes. J Neurosci 31:16125-16138.

Ku SP, Tolias AS, Logothetis NK, Goense J. 2011. fMRI of the face-processing network in the ventral temporal lobe of awake and anesthetized macaques. Neuron 70:352-362.

Lee JH, Durand R, Gradinaru V, Zhang F, Goshen I, Kim DS, Fenno LE, Ramakrishnan C, Deisseroth K. 2010. Global and local fMRI signals driven by neurons defined optogenetically by type and wiring. Nature 465:788-792.

Lim DH, Ledue J, Mohajerani MH, Vanni MP, Murphy TH. 2013. Optogenetic approaches for functional mouse brain mapping. Front Neurosci 7:54.

Lin MK, Nicolini O, Waxenegger H, Galloway GJ, Ullmann JF, Janke AL. 2013. Interpretation of medical imaging data with a mobile application: a mobile digital imaging processing environment. Front Neurol 4:85.

Ma D, Cardoso MJ, Modat M, Powell N, Wells J, Holmes H, Wiseman F, Tybulewicz V, Fisher E, Lythgoe MF, Ourselin S. 2014. Automatic structural parcellation of mouse brain MRI using multi-atlas label fusion. PLoS One 9:e86576.

Mai JK, Paxinos G, Voss T. 2008. Atlas of the Human Brain. San Diego: Elsevier Academic Press.

Majka P, Kublik E, Furga G, Wojcik DK. 2012. Common atlas format and 3D brain atlas reconstructor: infrastructure for constructing 3D brain atlases. Neuroinformatics 10:181-197.

Malkova NV, Gallagher JJ, Yu CZ, Jacobs RE, Patterson PH. 2014. Manganese-enhanced magnetic resonance imaging reveals increased DOI-induced brain activity in a mouse model of schizophrenia. Proc Natl Acad Sci USA 111:2492-2500.

Mikula S, Binding J, Denk W. 2012. Staining and embedding the whole mouse brain for electron microscopy. Nat Methods 9:1198-1201.

Miranda-Dominguez O, Mills BD, Grayson D, Woodall A, Grant KA, Kroenke CD, Fair DA. 2014. Bridging the gap between the human and macaque connectome: a quantitative comparison of global interspecies structure-function relationships and network topology. J Neurosci 34:5552-5563.

Morin LP, Wood RI. 2001. A Stereotaxic Atlas of the Golden Hamster Brain. San Diego: Academic Press.

Natt O, Watanabe T, Boretius S, Radulovic J, Frahm J, Michaelis T. 2002. High-resolution 3D MRI of mouse brain reveals small cerebral structures *in vivo*. J Neurosci Meth 120:203-209.

Neumann PE, Garretson JD, Skabardonis GP, Mueller GG. 1993. Genetic analysis of cerebellar folial pattern in crosses of C57BL/6J and DBA/2J inbred mice. Brain Res 619:81-88.

Nguyen H, McLachlan G, Cherbuin N, Janke A. 2014. False discovery rate control in magnetic resonance imaging studies via markov random fields. IEEE T Med Imaging *In Press.*

Papp EA, Leergaard TB, Calabrese E, Johnson GA, Bjaalie JG. 2014. Waxholm Space atlas of the Sprague Dawley rat brain. NeuroImage 97:374-386.

Pautler RG. 2004. *In vivo*, trans-synaptic tract-tracing utilizing manganese-enhanced magnetic resonance imaging (MEMRI). NMR Biomed 17:595-601.

Paxinos G, Franklin K. 2013. The Mouse Brain in Stereotaxic Coordinates. San Diego: Academic Press.

Paxinos G, Halliday G, Watson C, Koutcherov Y, Wang HQ. 2007. Atlas of the Developing Mouse Brain at E17.5, P0, and P6. San Diego: Elsevier Academic Press.

Paxinos G, Huang XF, Petrides M, Toga AW. 2009a. The Rhesus Monkey Brain in Stereotaxic Coordinates. San Diego: Elsevier Academic Press.

Paxinos G, Watson C. 1982. The Rat Brain in Stereotaxic Coordinates. San Diego: Academic Press.

Paxinos G, Watson C. 2014. Paxinos and Watson's The Rat Brain in Stereotaxic Coordinates. San Diego: Elsevier Academic Press.

Paxinos G, Watson C, Carrive P, Kirkcaldie MT, Ashwell K. 2009b. Chemoarchitectonic Atlas of the Rat Brain. San Diego: Elsevier Academic Press.

Paxinos G, Watson C, Petrides M, Rosa M, Tokuno H. 2012. The Marmoset Brain in Stereotaxic Coordinates. San Diego: Elsevier Academic Press.

Perez PD, Hall G, Kimura T, Ren Y, Bailey RM, Lewis J, Febo M, Sahara N. 2013. *In vivo* functional brain mapping in a conditional mouse model of human tauopathy (tauP301L) reveals reduced neural activity in memory formation structures. Mol Neurodegener 8:9.

Puelles L, Harrison M, Paxinos G, Watson C. 2013. A developmental ontology for the mammalian brain using the prosomere model. Trends Neurosci 36:570-578.

Puelles L, Martinez-de-la-Torre M, Paxinos G, Watson C, Martinez S. 2007. The Chick Brain in Stereotaxic Coordinates. An atlas featuring neuromeres and mammalian homologies. San Diego: Elsevier Academic Press.

Sforazzini F, Schwarz AJ, Galbusera A, Bifone A, Gozzi A. 2014. Distributed BOLD and CBV-weighted resting-state networks in the mouse brain. Neuroimage 87:403-415.

Sharief AA, Johnson GA. 2006. Enhanced T_2 contrast for MR histology of the mouse brain. Magn Reson Med 56:717-725.

Sheng M, Greenberg ME. 1990. The regulation and function of *c-fos* and other immediate early genes in the nervous system. Neuron 4:477-485.

Simmons DM, Swanson LW. 2009. Comparing histological data from different brains: Sources of error and strategies for minimizing them. Brain Res Rev 60:349-367.

Sled JG, Zijdenbos AP, Evans AC. 1998. A non-parametric method for automatic correction of intensity non-uniformity in MRI data. IEEE Trans Med Ima 17:87-97.

Spinelli S, Muller T, Friedel M, Sigrist H, Lesch KP, Henkelman M, Rudin M, Seifritz E, Pryce CR. 2013. Effects of repeated adolescent stress and serotonin transporter gene partial knockout in mice on behaviors and brain structures relevant to major depression. Front Behav Neurosci 7:215.

Steadman PE, Ellegood J, Szulc KU, Turnbull DH, Joyner AL, Henkelman RM, Lerch JP. 2014. Genetic effects on cerebellar structure across mouse models of autism using a magnetic resonance imaging atlas. Autism Res 7:124-137.

Stosiek C, Garaschuk O, Holthoff K, Konnerth A. 2003. *In vivo* two-photon calcium imaging of neuronal networks. Proc Natl Acad Sci USA 100:7319-7324.

Susaki EA, Tainaka K, Perrin D, Kishino F, Tawara T, Watanabe TM, Yokoyama C, Onoe H, Eguchi M, Yamaguchi S, Abe T, Kiyonari H, Shimizu Y, Miyawaki A, Yokota H, Ueda HR. 2014. Whole-brain imaging with single-cell resolution using chemical cocktails and computational analysis. Cell 157:726-739.

Tian L, Hires SA, Mao T, Huber D, Chiappe ME, Chalasani SH, Petreanu L, Akerboom J, McKinney SA, Schreiter ER, Bargmann CI, Jayaraman V, Svoboda K, Looger LL. 2009. Imaging neural activity in worms, flies and mice with improved GCaMP calcium indicators. Nat Methods 6:875-881.

Ullmann JF, Keller MD, Watson C, Janke AL, Kurniawan ND, Yang Z, Richards K, Paxinos G, Egan GF, Petrou S, Bartlett P, Galloway GJ, Reutens DC. 2012. Segmentation of the C57BL/6J mouse cerebellum in magnetic resonance images. NeuroImage 62:1408-1414.

Ullmann JF, Watson C, Janke AL, Kurniawan ND, Paxinos G, Reutens DC. 2014. An MRI atlas of the mouse basal ganglia. Brain Struct Funct 219:1343-1353.

Ullmann JF, Watson C, Janke AL, Kurniawan ND, Reutens DC. 2013b. A segmentation protocol and MRI atlas of the C57BL/6J mouse neocortex. NeuroImage 78:196-203.

Ullmann JFP, Cowin G, Kurniawan ND, Collin SP. 2010a. Magnetic resonance histology of the adult zebrafish brain: optimization of fixation and gadolinium contrast enhancement. NMR Biomed 23:341-346.

Ullmann JFP, Cowin G, Kurniawan ND, Collin SP. 2010b. A three-dimensional digital atlas of the zebrafish brain. NeuroImage 51:76-82.

Valdes-Hernandez PA, Sumiyoshi A, Nonaka H, Haga R, Aubert-Vasquez E, Ogawa T, Iturria-Medina Y, Riera JJ, Kawashima R. 2011. An *in vivo* MRI template set for morphometry, tissue segmentation, and fMRI localization in rats. Front Neuroinform 5:26.

Wang WH, Reutens DC, Yang Z, Nguyen G, Vegh V. 2014. Modified human contrast sensitivity function based phase mask for susceptibility-weighted imaging. NeuroImage Clin 4:765-778.

Watanabe T, Frahm J, Michaelis T. 2010. Myelin mapping in the living mouse brain using manganese-enhanced magnetization transfer MRI. NeuroImage 49:1200-1204.

Watanabe T, Tammer R, Boretius S, Frahm J, Michaelis T. 2006. Chromium (VI) as a novel MRI contrast agent for cerebral white matter: Preliminary results in mouse brain *in vivo*. Magn Reson Med 56:1-6.

Watson C, Paxinos G. 2010. Chemoarchitectonic Atlas of the Mouse Brain. San Diego: Elsevier Academic Press.

Wu G, Jia H, Wang Q, Shen D. 2011. SharpMean: groupwise registration guided by sharp mean image and tree-based registration. NeuroImage 56:1968-1981.

Wullimann MF, Rupp B, Reichert H. 1996. Neuroanatomy of the zebrafish brain: a topological atlas. Basel: Birkhäuser Verlag.

Yang Z, Richards K, Kurniawan ND, Petrou S, Reutens DC. 2012. MRI-guided volume reconstruction of mouse brain from histological sections. J Neurosci Meth 211:210-217.

Ying S, Wu G, Wang Q, Shen D. 2014. Hierarchical unbiased graph shrinkage (HUGS): a novel groupwise registration for large data set. NeuroImage 84:626-638.

Zhang J, Aggarwal M, Mori S. 2012. Structural insights into the rodent CNS via diffusion tensor imaging. Trends Neurosci 35:412-421.

Zhang X, Bearer EL, Perles-Barbacaru AT, Jacobs RE. 2010. Increased anatomical detail by *in vitro* MR microscopy with a modified Golgi impregnation method. Magn Reson Med 63:1391-1397.

Contrast Agent	Effect	Reference
Gadolinium	High magnetic moment and long electron relaxation times, efficiently shortens longitudinal and transverse relaxation times of solvent water protons.	(Caravan et al., 1999; Caravan, 2006; Ullmann et al., 2010a)
Chromium	Significantly increases contrast to noise ratios (CNR) by decreasing T_2 values in highly myelinated areas.	(Watanabe et al., 2006; Zhang et al., 2010; Chan et al., 2012)
Luxol Fast Blue	Increased longitudinal and transverse relaxation rates enabling high CNR to be obtained using T_1-weighted imaging.	(Blackwell et al., 2009)
Manganese	Enters cells via calcium channels and shortens T_1 values in tissues where it has collected.	(Natt et al., 2002; Pautler, 2004; Angenstein et al., 2007; Watanabe et al., 2010)
Myelin Imaging Compound	Dramatically shortens T_1, with high specificity for highly myelinated areas.	(Frullano et al., 2012)

Table 1. MRI-based contrast agents, their MR effects and some references.

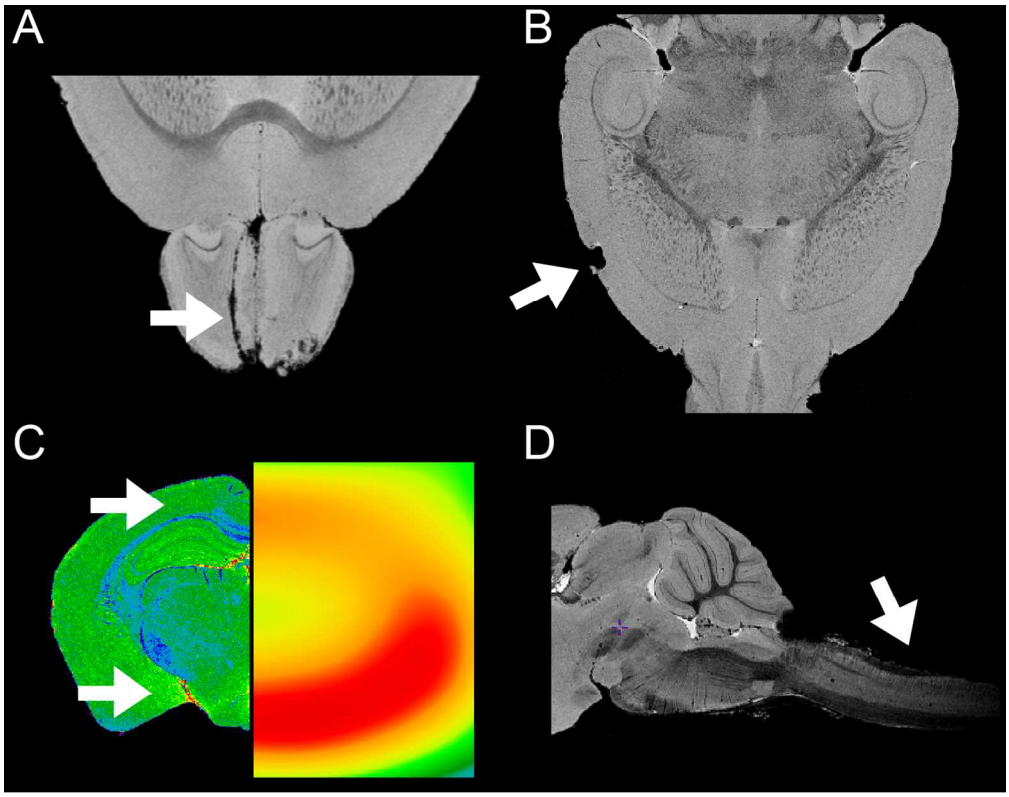

Figure 1. Examples of sample preparation and acquisition artifacts that should be controlled during pre-processing. Arrows indicate: a) dissection artifact in the olfactory bulb as a result of surgical damage during extraction of cortex; b) signal drop out due to air bubble on surface of neocortex; c) B0 inhomogeneity - on the right is the extracted B0 inhomogeneity field, on the left is the uncorrected image with a spectral colourmap (note the change in signal intensity between the top and bottom of the cortex (arrows) in tissue that would normally exhibit constant signal); d) signal drop off as a result of distance from the receive coil. 127x100mm (300 x 300 DPI)

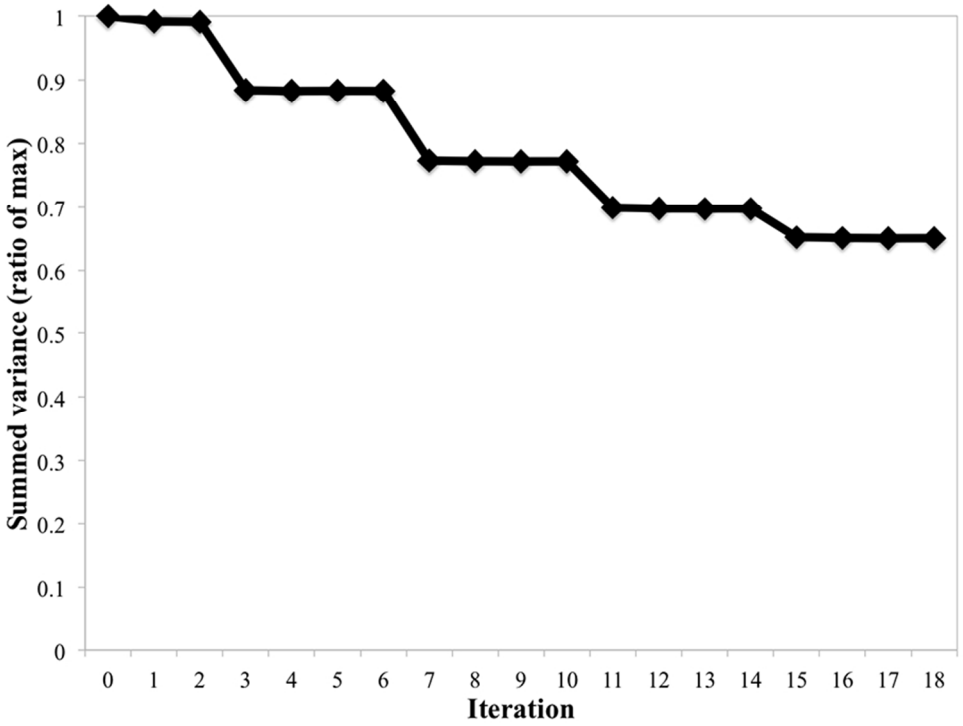

Figure 2. Plot of voxel level variance summed across the brain as compared to iteration

Note that as the iteration count increases, the residual variance is decreased. The step like appearance of the plot is due to finer fit criteria being introduced every four iterations.
80x57mm (300 x 300 DPI)

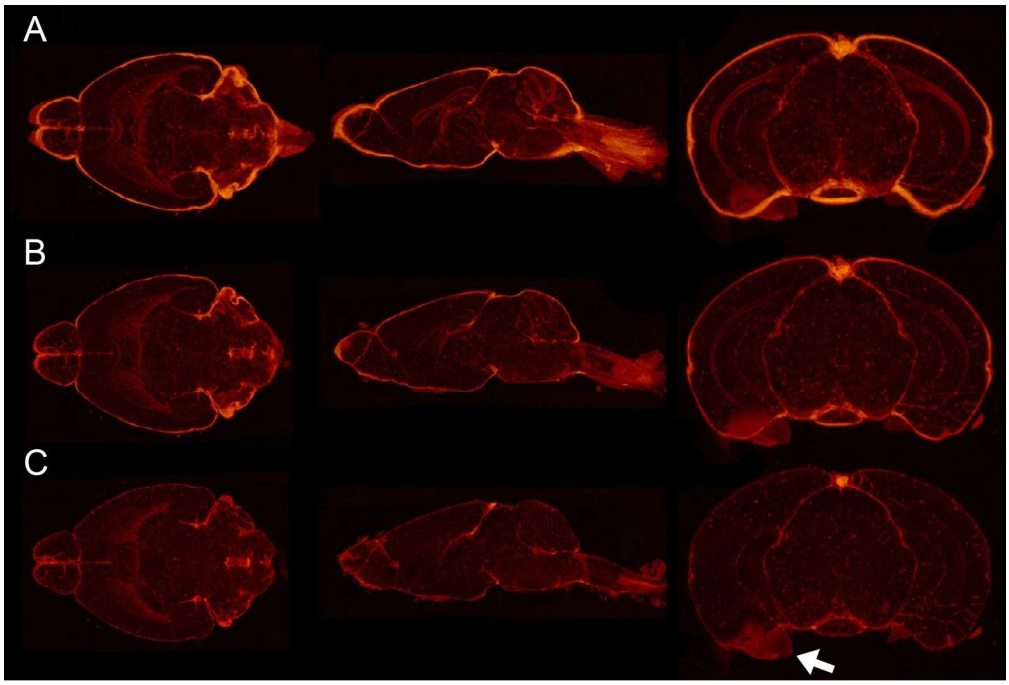

Figure 3. Standard deviation images at three points during the averaging process. A) Initial linear model; B) 8th generation nonlinear model; C) 21st generation nonlinear model. The reduction in hyperintense voxels demonstrates a reduction in variance as the model building progresses. The arrow indicates the result of a single individual with a large distortion in the left cortical amygdaloid area as a result of susceptibility. With a robust averaging procedure this feature will be down-weighted in the final model as the variance for this point is greater than the average.
169x114mm (300 x 300 DPI)

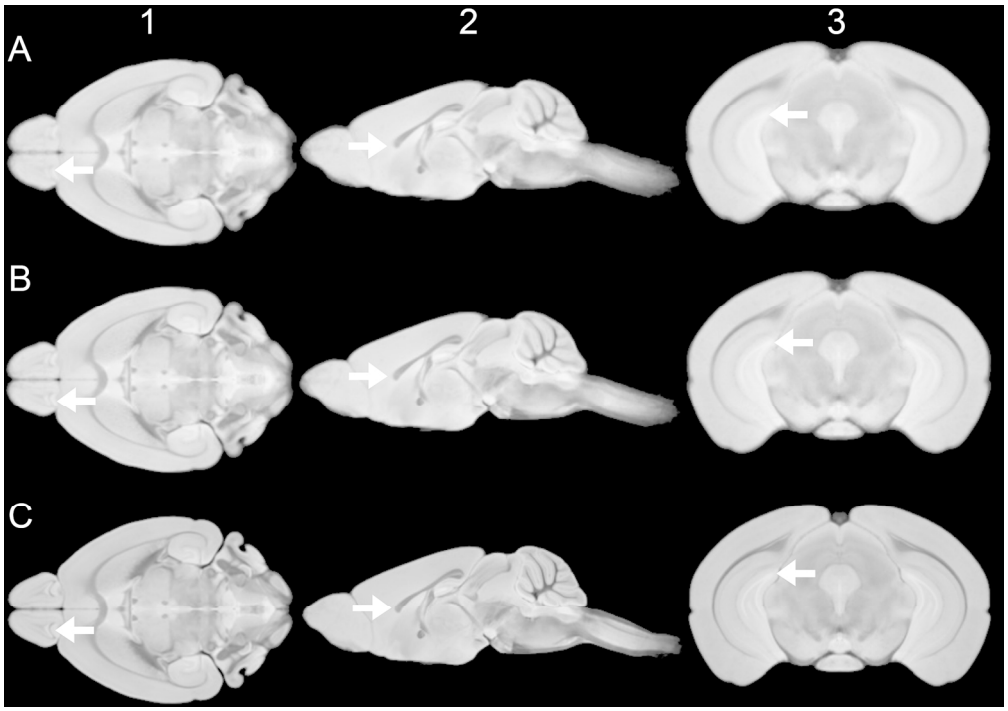

Figure 4. Comparison of structural delineation in an evolving model of symmetric structure in mouse. a) Initial linear model; b) 8th generation nonlinear model; c) 21st generation nonlinear final model. Note how structures and cellular layers become progressively easier to identify; examples are the internal plexiform layer of the olfactory bulb (1), the genu of the corpus callosum (2), and the granule cell layer of the dentate gyrus (3).
171x120mm (300 x 300 DPI)

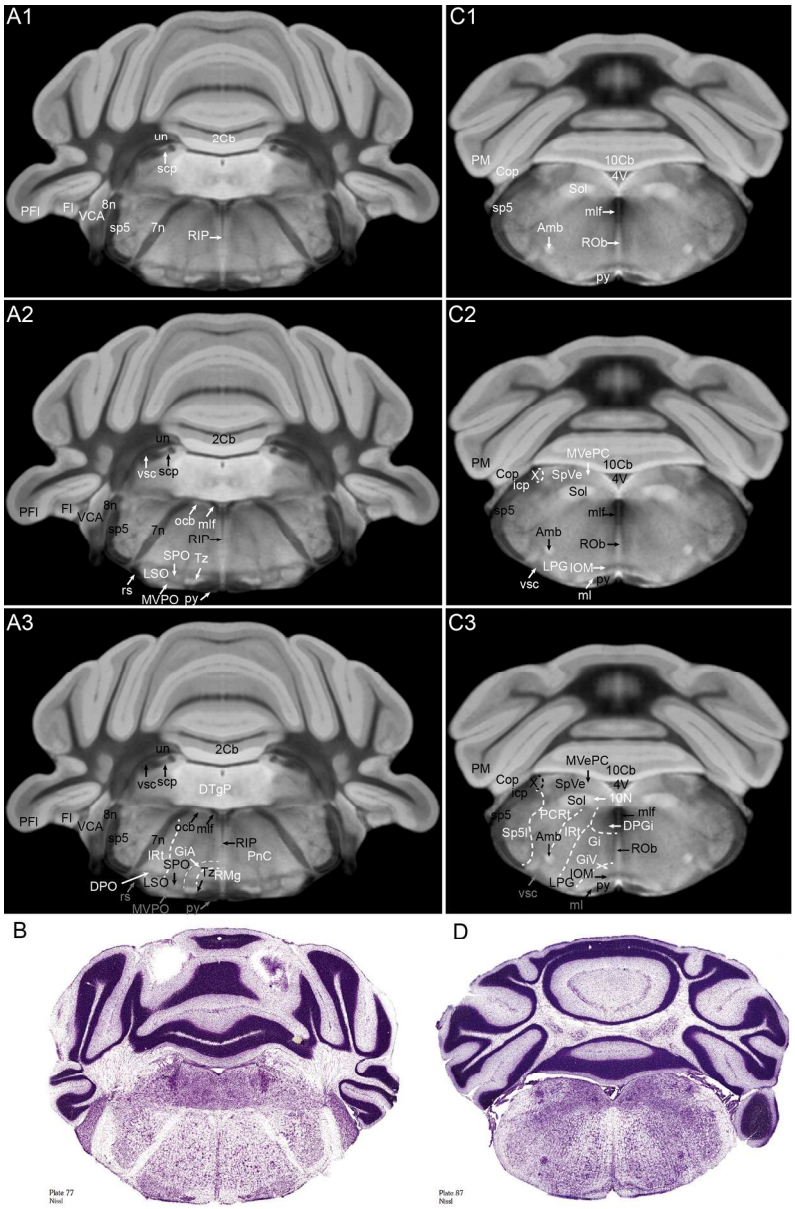

Figure 5. Sample segmentation of the mouse C57BL/6J brain stem. Segmentation of MRI slices through the rostral end of the brain stem (A) and the caudal end of the brain stem (C). Only the left side was segmented to allow for examination of structures on right side of the brain. Delineation of structures occurs in a progressive manor (A1-A3, C1-C3) with newly identified structures appearing in white and previously identified structures appear in black/gray. Histological sections (B, D) best matching the MRI slices are shown from the Paxinos and Franklin mouse brain histology atlas (Paxinos and Franklin 2013). 10Cb, lobule 10 of the cerebellar vermis; 10N, dorsal motor nucleus of vagus; 2Cb, lobule 2 of the cerebellar vermis; 4V, 4th ventricle; 7n, facial nerve; 8n, vestibulocochlear nerve; Amb, ambiguus nucleus; Cop, copula of pyramis; DPGi, dorsal paragigantocellular nucleus; DPO, dorsal periolivary region; DTgP, dorsal tegmental nucleus, pericentral part, Fl, flocculus; Gi, gigantocellular reticular nucleus; GiA, gigantocellular reticular nucleus, alpha part; GiV, gigantocellular reticular nucleus, ventral part; icp, inferior cerebellar peduncle; IOM, inferior olive, medial nucleus; IRt, intermediate reticular nucleus; LPG, lateral paragigantocellular nucleus; LSO, lateral superior olive; ml, medial lemniscus; mlf, medial longitudinal fasciculus; MVePC,

medial vestibular nucleus; parvicellular part; MVPO, medioventral periolivary nucleus; ocb, olivocochlear bundle; PCRt, parvicellular reticular nucleus; PFl, paraflocculus; PM, paramedian lobule; PnC, pontine reticular nucleus, caudal part; py, pyramindal tract; RIP, raphe interpositus nucleus; RMg, raphe magnus nucleus; ROb, raphe obscurus nucleus; rs, rubrospinal tract; scp, superior cerebellar peduncle; Sol, solitary nucleus; sp5, spinal trigeminal tract; Sp5I, spinal trigeminal nucleus, interpolar part; SPO, superior paraolivary nucleus; SpVe, spinal vestibular nucleus; Tz, nucleus of the trapezoid body; un, uncinate fasciculus of the cerebellum; VCA, ventral cochlear nucleus, anterior part; vsc, ventral spinocerebellar tract; X, nucleus X.
150x230mm (300 x 300 DPI)

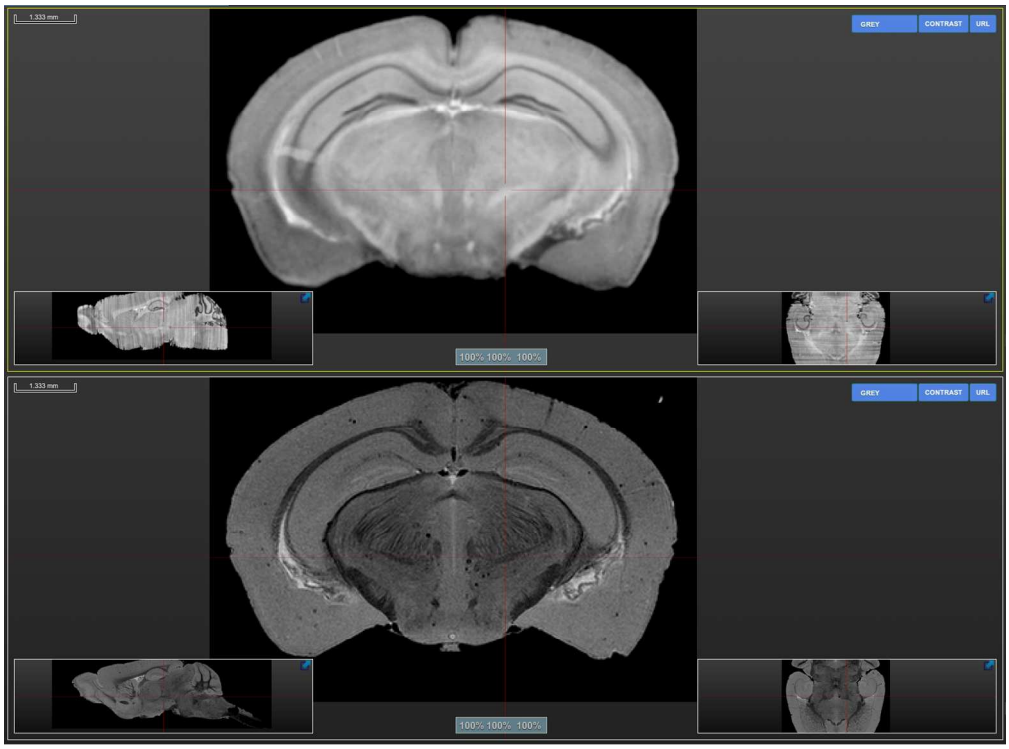

Figure 6. Registration and visualization of MRI and histological data sets using TissueStack. Tissuestack visualization software allows registered histological (top) and MRI (bottom) data sets to be viewed simultaneously with crosshairs indicating the same location/structure in each dataset.
140x104mm (300 x 300 DPI)

It is now possible to make quality brain atlases based on MR images. The value of these atlases can be increased by the use of multiple data sets, modern nomenclature, segmentation of a minimum deformation model, and sophisticated dissemination strategies.

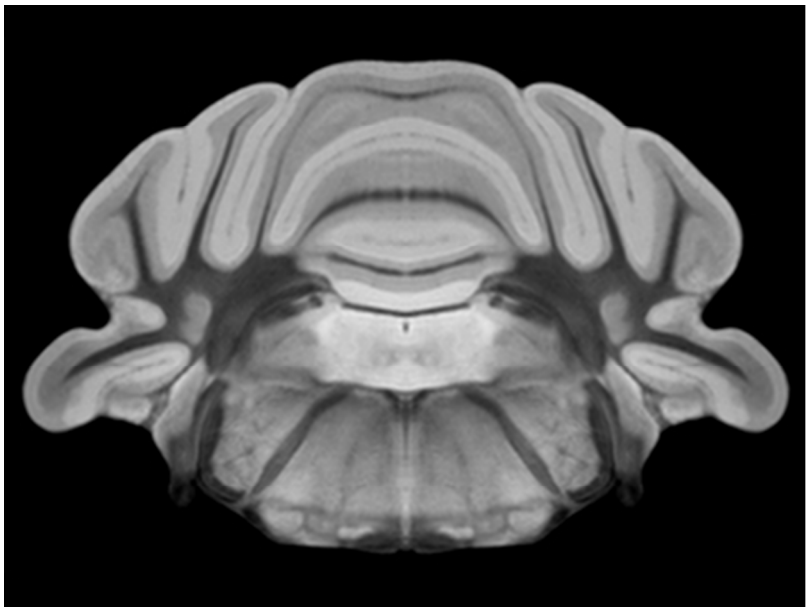

High resolution MR image of mouse hindbrain
141x105mm (72 x 72 DPI)